Fault Severity Estimation in Cracked Shafts by Integration of Phase Space Topology and Convolutional Neural Network

Utkarsh Andharikar[1], Amirhassan Abbasi[2], Prashant Kambali[3] and C. Nataraj[4]

[1,2,3,4] *Villanova Center for Analytics of Dynamic Systems, Villanova University, Villanova, PA 19085, USA*
uandhari@villanova.edu
aabbasi@villanova.edu
prashant.kambali@villanova.edu
nataraj@villanova.edu

ABSTRACT

With the rapid advancement of industrial systems and the unavoidable complications and interconnectedness in systems, diagnostics of industrial machinery are achieving paramount importance. Accurate estimation of health condition of industrial machinery becomes more challenging due to the inherent nonlinearity, complexity, and uncertainty of the observations. Nonlinear dynamic analysis has proven to be a powerful tool for providing information about the health condition of a system that can be used for diagnostic applications. The current study particularly focuses on crack depth estimation using phase space analysis. Phase space provides a topological representation of the dynamics of the system and is highly informative about the health condition. The information suitable for diagnostics is employed by Convolutional Neural Networks, which are known to be powerful in extracting spatial information from maps. The proposed diagnostic method is evaluated on a Jeffcott rotor model with transverse crack in the rotating shaft to estimate the severity of the fault from the phase space topology as a case study.

1. INTRODUCTION

Predicting the health of machinery is becoming of paramount importance as the complications and interconnections in systems is increasing. It is difficult to predict the exact working condition of the machinery due to the inherent complexity and the dynamical behavior of the measured outputs.

Detecting cracks in rotating shafts in industrial settings is exceptionally challenging due to the rapid progression of the crack, often leading to machine failure with little warning. This difficulty is due to the nonlinear effects imparted by opening and closing of the crack (Nelson & Nataraj, 1986; Shudeifat & Nataraj, 2020; Alzarooni, Al-Shudeifat, Shiryayev, & Nataraj, 2020). In all rotating systems two speeds are important: the operating speed and the critical speed. Changes in the frequencies of 1X, 2X, 3X components of the rotating speeds which are in fraction of critical speed are well known for detecting cracks in rotating systems (Imam, Azzaro, Bankert, & Scheibel, 1989; Sekhar, 2005; Gasch, 1993). Various time frequency domain methods like Hilbert Huang Transform (HHT) (Li, Zhang, & He, 2012; D. Guo & Peng, 2007), Wavelet analysis (L. Lin & Chu, 2012; Gómez, Castejón, & García-Prada, 2016), Short Time Fourier Transform (STFT) (Chandra & Sekhar, 2016) etc. are used for detecting cracks using transient vibrations of rotor shaft. Nevertheless, owing to inherent nonlinearities and varying operating conditions, the task of accurately estimating the depth of cracks in a rotating shaft remains an unresolved issue to this day.

The term 'phase space' refers to collection of all possible states of a physical system. These states encompass both the system's positions and momenta, which are essential for predicting its future behavior. Thus the topology of phase space not only characterizes the system's dynamics but also provides a visual depiction of all attainable states that the system can undergo.

Previously this pictorial representation was given a quantitative form by transforming it into probability density function to help diagnose the condition of a system (Samadani, Kwuimy, & Nataraj, 2016; Mohamad & Nataraj, 2020; Mohamad, Nazari, & Nataraj, 2019; Carroll, 2015). Unlike the previous methods based on phase space topology (PST) which require hand crafted features, we rely on the machine learning method, specifically CNNs, to select relevant features for mapping the input space to the output space. CNN have been used for time series classification just by using 1D signals (Abdel-Hamid, Mohamed, Jiang, & Penn, 2012; Zheng, Liu, Chen, Ge, & Zhao, 2014; Ince, Kiranyaz, Eren,

Askar, & Gabbouj, 2016; Mohamad, Abbasi, Kim, & Nataraj, 2021; Acharya, Oh, Hagiwara, Tan, & Adeli, 2018) or by converting the time series to image representations like recurrence plots (Debayle, Hatami, & Gavet, 2018), spectrogram (Khan, Ko, Lim, & Kim, 2019; Raghu, Sriraam, Temel, Rao, & Kubben, 2020), wavelet maps (Shao, McAleer, Yan, & Baldi, 2019), Markov Transition Fields, Grammian Angular Fields (Wang, Oates, et al., 2015; Wang & Oates, 2015) etc. In rotordynamics orbit shape plays an important role in determining the operating condition of the system and CNNs have been used to classify the orbit shapes to determine various faults such as imbalance, oil whirl, rubbing, misalignment etc. in a rotor system (Caponetto, Rizzo, Russotti, & Xibilia, 2019; Wu, Feng, Sun, Xu, & Ai, 2019; Jiang, Wang, Zhao, Xu, & Lin, 2020).

In this paper we have attempted to predict the extent of damage by predicting the crack depth, instead of classifying it, in a rotating shaft. We employ CNNs to distinguish the phase portraits of dynamics of a cracked shaft exhibiting parametric excitation due to crack-induced stiffness variation. Additionally, the Global Average Pooling (GAP) layer is used instead of fully connected layer at the end of CNN to help in visualization of learned kernels, and identify distinguishing regions of phase space which can in future studies help to handcraft robust features for crack depth estimation.

In the following sections the equations of motion are described from which phase space images are generated, the structure of CNN and the procedure to generate activation maps are described in Section 3. The results obtained from CNN are presented in Section 4 and finally the discussion on the regions of phase space to which the CNN gives relative importance is presented in Section 5.

2. EQUATIONS OF MOTION

We consider a simple two degree of freedom rotor model as shown in Fig. 1 with the following equations of motion (Abbasi, Nazari, & Nataraj, 2020; Patel & Darpe, 2008):

$$\begin{aligned} m\ddot{V} + c\dot{V} + k_Y V + k_{YZ} V &= m\varepsilon\omega^2 \sin(\theta+\beta) \\ m\ddot{W} + c\dot{W} + k_{ZY} W + k_Z W &= m\varepsilon\omega^2 \cos(\theta+\beta) - mg \end{aligned} \tag{1}$$

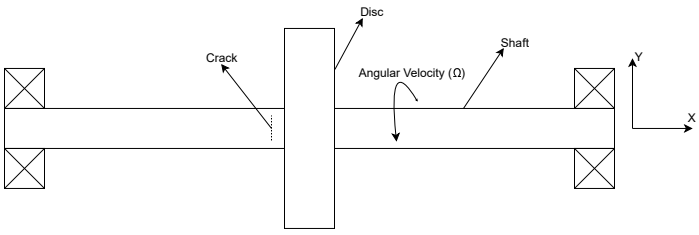

Figure 1. Schematic of the rotor

The assumptions for the model are as follows. 1. Linear viscous damping is assumed; 2. Transverse vibrations are predominant and torsional, axial vibrations are negligible; 3. depth of crack is constant; and, 4. the zone of operation is well below yield stress, hence linear elastic mechanics is valid. Using Eq. 1 and the values of the parameters from (Patel & Darpe, 2008), the time response is simulated to obtain the phase portraits at varying crack depths.

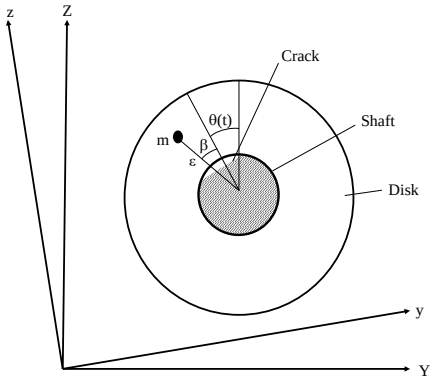

Figure 2. Reference axes for the rotor

The effect of crack on the stiffness and cross stiffness terms is incorporated using an appropriate breathing function in rotating coordinates which can be transformed to fixed coordinates using a coordinate transformation. When a rotor rotates, the crack opening and closing varies as per the rotation angle $\theta(t)$, thus simultaneously varying the stiffness. This variation is incorporated using a breathing function for which we simply follow the model from (Patel & Darpe, 2008). The effect of weight is assumed to be much higher than unbalance force. We have used the following Eq. 2 as the breathing function which is reasonably valid for behaviour of the system for crack depths up to $0.25D$ (Gasch, 2008).

$$F(\theta) = \frac{1}{2}(1+\cos(\theta)) \tag{2}$$

After rearranging Eq. 1 in matrix form and including the stiffness coupling and model variation in flexibility due to the action of the crack, we get the following.

$$\begin{bmatrix} k_y & k_{yz} \\ k_{zy} & k_z \end{bmatrix} = \begin{bmatrix} k_0 & 0 \\ 0 & k_0 \end{bmatrix} - F(\theta) \begin{bmatrix} S_{11} & S_{12} \\ S_{21} & S_{22} \end{bmatrix} \tag{3}$$

Here, $\begin{bmatrix} k_y & k_{yz} \\ k_{zy} & k_z \end{bmatrix}$ are related to $\begin{bmatrix} k_Y & k_{YZ} \\ k_{ZY} & k_Z \end{bmatrix}$ by standard coordinate transformation matrices. The terms . Also, $\begin{bmatrix} S_{11} & S_{12} \\ S_{21} & S_{22} \end{bmatrix}$ is the stiffness contribution of crack to the rotor. To derive the stiffness terms of the cracked rotor, Fig. 3 (Abbasi, Nazari, & Nataraj, 2022) shows the section of the cracked shaft with details: a, e, D are the crack depth, crack width and shaft

diameter respectively, while a_0 and e_0 are their initial values. The relation between the shaft diameter and the crack depth

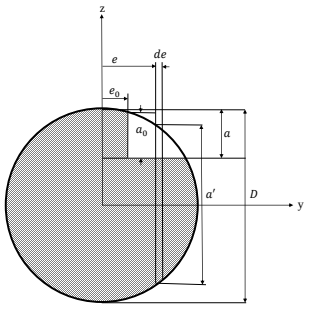

Figure 3. Cross section view of shaft with crack dimensions

can be shown by using a parameter $a' = \sqrt{D^2 - (2e)^2}$. Then the elements of S in Eq. 3 are computed as follows.

$$\begin{aligned} S_{11} &= k_0 - \frac{\hat{g_y}}{\hat{g_y}\hat{g_z} - \hat{g}_{zy}^2}, \\ S_{22} &= k_0 - \frac{\hat{g_y}}{\hat{g_y}\hat{g_z} - \hat{g}_{yz}^2}, \\ S_{12} &= S_{21} = -\frac{\hat{g_{zy}}}{\hat{g_{yy}}\hat{g_{zz}} - \hat{g}_{zy}^2} \end{aligned} \tag{4}$$

where,

$$\begin{aligned} g_z &= \frac{L^3}{48EI} + \iint \frac{128L^2a'^2a}{E\pi D^8} F\left(\frac{a}{a'}\right)^2 da\,de \\ g_y &= \frac{L^3}{48EI} + \iint \frac{512L^2e^2a}{E\pi D^8} F'\left(\frac{a}{a'}\right)^2 da\,de \\ g_{yz} &= g_{zy} = \iint \frac{256L^2a'^2ae}{E\pi D^8} F\left(\frac{a}{a'}\right) F'\left(\frac{a}{a'}\right) da\,de \end{aligned} \tag{5}$$

and,

$$\begin{aligned} F\left(\frac{a}{a'}\right) &= \sqrt{\left(\frac{2a'}{\pi a}\right)\tan\left(\frac{\pi a}{2a'}\right)} \\ &\frac{0.923 + 0.199\left[1 - \sin(\frac{\pi a}{2a'})\right]^4}{\cos(\frac{\pi a}{2a'})} \\ F'\left(\frac{a}{a'}\right) &= \sqrt{\left(\frac{2a'}{\pi a}\right)\tan\left(\frac{\pi a}{2a'}\right)} \\ &\frac{0.752 + 2.02\left(\frac{a}{a'}\right) + 0.37\left[1 - \sin(\frac{\pi a}{2a'})\right]^3}{\cos(\frac{\pi a}{2a'})} \end{aligned} \tag{6}$$

g_y, g_z, g_{zy}, g_{yz} are the direct and cross coupled flexibility coefficients respectively. When they are integrated for the depth of the fully open crack we get the terms $\hat{g_y}$, $\hat{g_z}$, $\hat{g_{zy}}$, $\hat{g_{yz}}$, $\hat{g_{yy}}$, $\hat{g_{zz}}$ and the corresponding stiffness terms in Eq. 4 (Patel & Darpe, 2008; Abbasi et al., 2020).

Parameters from (Patel & Darpe, 2008) are used for simulation and are as follows: $L = 0.7\ m$, $D = 45\ mm$, $m = 25\ kg$, $\varepsilon = 5\ \mu m$, $\beta = 1.5708\ rad$, $c = 972.86\ kg/s$, $\frac{mg}{k_0} = 4.147 \times 10^{-5}\ m$. The appearance of subharmonic and superharmonic frequencies is a well-known feature of the output response of a rotating shaft with crack. Let us consider a parameter $\lambda = \frac{\omega}{\sqrt{k_0/m}}$ to indicate the operating speed with respect to the critical speed. We have considered the $(3/10)^{th}$ of critical speed (i.e., $\lambda = 0.3$), to obtain the time series data. The frequencies are normalized with respect to the operating speed ω. The extent of crack progression is generally specified as percentage of shaft diameter (D). Here we are simulating the system for crack depths ranging from 2.2% to 32.5% of shaft diameter (D). Continuous variation of fault here imparts a notion of progressive increase in its severity. The corresponding phase portraits of the rotor shaft with increasing crack depths for noise free signal are shown in Fig. 4.

3. CONV NETS

Following the success of AlexNet (Krizhevsky, Sutskever, & Hinton, 2017, 2012), deep CNNs gained widespread popularity for tasks related to image classification. CNNs offer distinct advantages over simple feedforward neural networks when processing multidimensional representations, as they can learn and extract meaningful abstractions without the need for explicit handcrafted features. The utilization of CNNs is particularly advantageous for capturing temporal and spatial correlations (Lecun, Bottou, Bengio, & Haffner, 1998) within a topological structure, providing qualitative insights into dynamical systems. Comparing a feedforward network and a CNN of similar size, the latter exhibits fewer parameters and connections, making them more trainable. Although this reduction in parameters may lead to a slight degradation in overall network accuracy, it remains acceptable. Figure 5 shows the schematic of the CNN used.

3.1. Visualizing CNN

It is challenging to visualize what a neural network has learned, especially after the first convolutional layer, due to the difficulty in inverting the features back to the pixel space. This challenge is further compounded when there is a fully connected layer following the convolutional filters. To address this issue, Zhou et al. (B. Zhou, Khosla, Lapedriza, Oliva, & Torralba, 2016) extended the concept of global average pooling layer introduced by Lin et al. (M. Lin, Chen, & Yan, 2013) to replace the fully connected layers at the end of the network. This modification enables accurate discriminative localization, producing activation maps that highlight the relative importance of the learned features in the input image

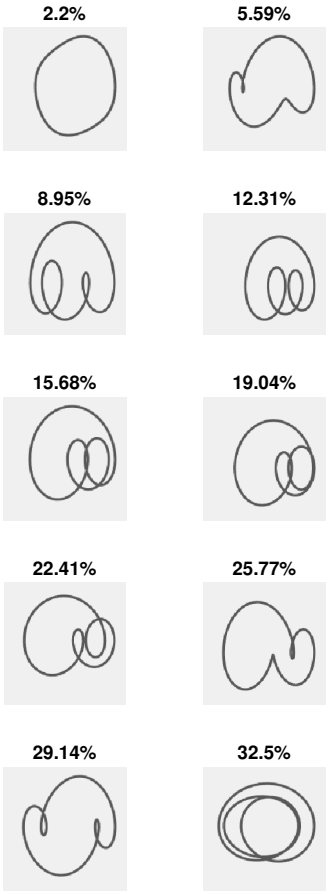

Figure 4. Phase portraits for varying crack depth ratios expressed as percent of shaft diameter.

for generating a specific output. While Zhou et al. (B. Zhou et al., 2016) initially applied this technique to CNNs using softmax classification, it has been extended for regression layer in subsequent works (Wang & Yang, 2017; X. Zhou, Jin, Shang, & Guo, 2020).

In this study, we present a concise methodology for generating these activation maps in our specific case. For 'N' feature maps i.e., $n = 1...N$, the average activation in the last global average pooling layer will be,

$$\Phi_n = \sum_{i,j} I_n(i,j) \tag{7}$$

$$\hat{\psi} = \sum_{n=1}^{N} \alpha_n \Phi_n \tag{8}$$

The output of Eq. 8 is input to the final regression layer to compute the mean square error to be minimized. Thus, the activation maps can be formulated as:

$$A_n = \sum_{n=1}^{N} \alpha_n I_n(i,j) \tag{9}$$

Here α_n represents the connection weight from each neuron of global average pooling layer to the output neuron. As the final layer is average pooling we can get the weighted sum of all the filters of penultimate layer i.e., the last convolution layer to get an activation map as per Eq. 9. This activation map after upsampling will show the relative importance of the spatial regions in estimating the required output of the CNN.

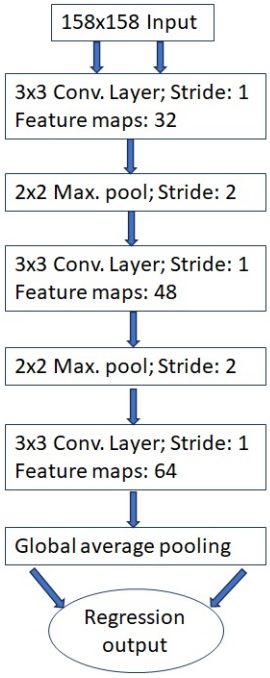

Figure 5. Structure of network

4. METHODOLOGY

Using Bayesian optimization, the structure for the CNN shown in Fig. 5 and its corresponding hyperparameters were obtained to achieve the lowest root mean square (RMS) error on the training set. Prior to training, all input images were preprocessed by scaling them within the range of 0 to 1. Stochastic gradient descent was employed to update the weights during the training process. Additionally, batch normalization and ReLU activation functions were applied after each convolutional layer and before the pooling operation. The hardware platform with the processor Intel i7-11700 and graphics card type Nvidia Quadro P620 respectively were used and MATLAB 2021a DeepLearning Toolbox was employed as the software package for training and testing of the network. Although entire multidimensional phase space can

be used in a CNN we are using only the trajectories lying in the V,$\dot{V}$ plane of the system (Eq. 1) to train the CNN. For each crack depth ratio, ranging from 2.2% to 32.5%, a total of 180 phase space images are generated for training dataset, while 60 images are included in the the validation and testing dataset. The data distribution corresponding to 10 different crack depths is presented in Table 1.

Table 1. Data division for CNN

Train data	Validation data	Test data
1800	600	600

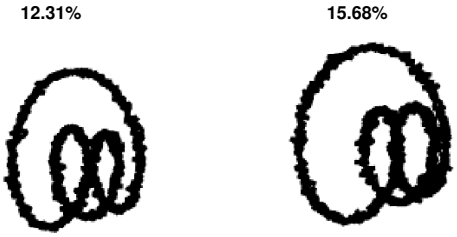

Figure 6. Phase portraits corresponding to 25dB SNR and the crack depth to diameter ratio of 12.31% (on left) and 12.68% (on right) respectively.

After training the network on noise free data, the network was tested for noisy data by gradually increasing signal to noise ratio (SNR). The number of samples for noisy test data were similar to the noise free case as shown in Table 1 and a sample of the phase portraits of signals corrupted at 25dB SNR are shown in Fig. 6.

Table 2. RMS Error.

	R value	**RMSE**
Without noise	0.9972	0.0169
With 45dB noise	0.9341	0.0153
With 40dB noise	0.8413	0.0157
With 35dB noise	0.5441	0.0190
With 30dB noise	-0.2962	0.0309
With 25dB noise	-0.3561	0.0465

5. RESULTS AND DISCUSSION

Figures 7 and 8 depicts the activation maps representing the phase portraits for noise free and noisy signals. It can be observed from the figures that the relative importance is assigned by the preceding convolutions to different regions of phase space for accurately estimating the crack depth. The bright regions indicate the most important pixels while the darker regions are comparatively less important. The brightness patterns i.e., the activations of kernel are of varying in-

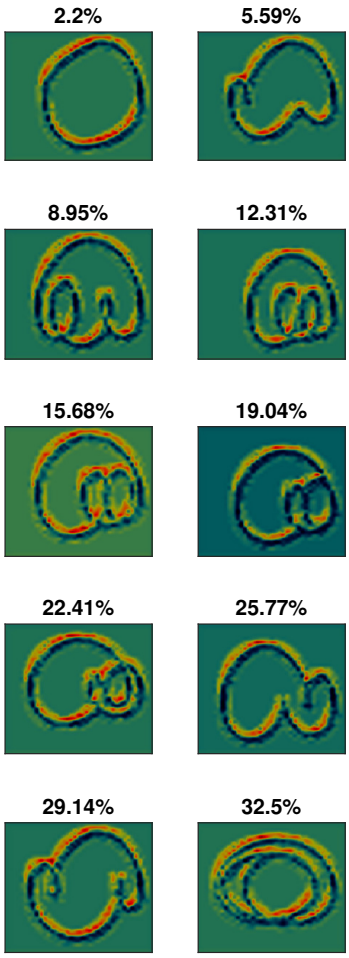

Figure 7. Activation maps for various phase portraits corresponding to crack depth to diameter ratio as given in Fig. 4 for noise free condition.

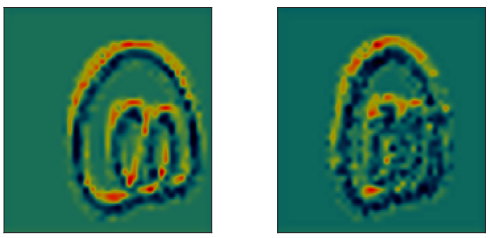

Figure 8. Activation maps for phase portraits corresponding to crack depth to diameter ratio of 12.31% with 25dB added noise on the right and noise free case on the left.

tensities along the edges of the phase portraits. Besides edges activations are always higher in places where the phase portrait curves or forms a loop.

Based on experimental observations and the general theory of nonlinear dynamics, it is well-established that the extent of a fault is influenced by the diameter of closed loops in the phase space. Furthermore, the presence of additional harmonics induced by parametric excitation can lead to the formation of loops in phase portraits (Abbasi et al., 2022; C. Guo et al., 2013). Taking these observations into account, it can be inferred that the network aims to extract qualitative spatial information from the phase space of the system, which is indicative of the changing dynamics induced by the faults. The RMS error values for estimation of crack depth for the cases of noise free and noisy signals are documented in Table 2. The proposed method performs well for noise free signal with RMSE 0.0169. However, the performance deteriorates slightly with added noise for SNR ranging from 45dB to 25dB which can be observed by the increasing RMSE values ranging from 0.0169 to 0.0465. The coefficient of regression (R) value drops considerably after decreasing SNR below 35dB.

6. CONCLUSION

Machine learning methods continue to evolve and are progressively being applied to real world systems. In this work we are proposing a machine learning method to estimate the crack depth of a rotating shaft. The proposed method uses CNN trained with images of phase portraits that represents the varying dynamics of cracked rotor shaft for different crack depths. The hyperparameters of CNN are optimized using Bayesian optimization technique. The trained CNN learns distinguishing features from qualitative representations of a dynamical system. This is indicated by the activation map of the phase portrait to estimate the required crack depth. The regions highlighted not only confirms the previous understanding from theory and experiments but can possibly give newer insights about the dynamics of complex nonlinear systems. The proposed method estimates the crack depth with RMSE of 0.0169 without noise. To represent the real world situations the proposed method is also tested with noisy signal for different SNR ranging from 45dB to 25dB. The method consistently demonstrated better performance with RMSE ranging from 0.0153 to 0.0465 for different noise ratios. The RMS error reported indicates the robustness of proposed method to estimate the crack depth, highlighting its potential as a valuable tool for detecting crack depths within industrial applications.

ACKNOWLEDGMENT

This project was supported by a grant from Office of Naval Research (Grant No. N00014-22-1-2480). We are grateful to ONR and Capt. Lynn Petersen for recognizing the importance of this work.

NOMENCLATURE

a	Instantaneous crack depth
c	Linear viscous damping
D	Shaft diameter
e	Embedded dimension
g	Acceleration due to gravity
k_0	Direct stiffness of uncracked shaft in rotating frame
k_Y	Direct stiffness of cracked shaft along Y direction in stationary reference frame
k_Z	Direct stiffness of cracked shaft along Z direction in stationary reference frame
k_{YZ}	Cross stiffness of cracked shaft along Y direction in stationary reference frame
k_{ZY}	Cross stiffness of cracked shaft along Z direction in stationary reference frame
m	Mass of disc and shaft
V	Displacement of cracked rotor shaft along Y direction
e	Instantaneous crack width
W	Displacement of cracked rotor shaft along Z direction
β	Angle at which unbalance force acts
ε	Eccentricity in rotor shaft
λ	Ratio of operating speed to first critical speed of healthy system
θ	Instantaneous angular displacement at time t
ω	Angular velocity
Φ_n	Output of n^{th} feature map from last conv. layer to global average pooling layer.
α_n	connection weight of layer connecting GAP to output neuron.

REFERENCES

Abbasi, A., Nazari, F., & Nataraj, C. (2020). On modeling of vibration and crack growth in a rotor for prognostics. In *In proceedings of the annual conference of the phm society 2020* (Vol. 12). Retrieved from https://doi.org/10.36001/phmconf.2020.v12i1.1193

Abbasi, A., Nazari, F., & Nataraj, C. (2022, dec). Adaptive modeling of vibrations and structural fatigue for analyzing crack propagation in a rotating system. *Journal of Sound and Vibration*, *541*, 117276. doi: 10.1016/j.jsv.2022.117276

Abdel-Hamid, O., Mohamed, A.-r., Jiang, H., & Penn, G. (2012). Applying convolutional neural networks concepts to hybrid nn-hmm model for speech recognition. In *2012 ieee international conference on acoustics,*

speech and signal processing (icassp) (p. 4277-4280). doi: 10.1109/ICASSP.2012.6288864

Acharya, U. R., Oh, S. L., Hagiwara, Y., Tan, J. H., & Adeli, H. (2018, sep). Deep convolutional neural network for the automated detection and diagnosis of seizure using EEG signals. *Computers in Biology and Medicine*, *100*, 270–278. doi: 10.1016/j.compbiomed.2017.09.017

Alzarooni, T., Al-Shudeifat, M. A., Shiryayev, O., & Nataraj, C. (2020, oct). Breathing crack model effect on rotor's postresonance backward whirl. *Journal of Computational and Nonlinear Dynamics*, *15*(12). doi: https://doi.org/10.1115/1.4048358

Caponetto, R., Rizzo, F., Russotti, L., & Xibilia, M. G. (2019). Deep learning algorithm for predictive maintenance of rotating machines through the analysis of the orbits shape of the rotor shaft. In *Proceedings of the 1st international conference on smart innovation, ergonomics and applied human factors (SEAHF)* (pp. 245–250). Springer International Publishing. doi: 10.1007/978-3-030-22964-1_25

Carroll, T. L. (2015, jan). Attractor comparisons based on density. *Chaos: An Interdisciplinary Journal of Nonlinear Science*, *25*(1), 013111. doi: 10.1063/1.4906342

Chandra, N. H., & Sekhar, A. (2016, may). Fault detection in rotor bearing systems using time frequency techniques. *Mechanical Systems and Signal Processing*, *72-73*, 105–133. doi: https://doi.org/10.1016/j.ymssp.2015.11.013

Debayle, J., Hatami, N., & Gavet, Y. (2018, apr). Classification of time-series images using deep convolutional neural networks. doi: 10.1117/12.2309486

Gasch, R. (1993, jan). A survey of the dynamic behaviour of a simple rotating shaft with a transverse crack. *Journal of Sound and Vibration*, *160*(2), 313–332. doi: 10.1006/jsvi.1993.1026

Gasch, R. (2008). Dynamic behaviour of the laval rotor with a transverse crack. *Mechanical Systems and Signal Processing*, *22*(4), 790-804. Retrieved from https://doi.org/10.1016/j.ymssp.2007.11.023 (Special Issue: Crack Effects in Rotordynamics)

Gómez, M., Castejón, C., & García-Prada, J. (2016, feb). Crack detection in rotating shafts based on 3 × energy: Analytical and experimental analyses. *Mechanism and Machine Theory*, *96*, 94–106. doi: https://doi.org/10.1016/j.mechmachtheory.2015.09.009

Guo, C., AL-Shudeifat, M., Yan, J., Bergman, L., McFarland, D., & Butcher, E. (2013, aug). Application of empirical mode decomposition to a jeffcott rotor with a breathing crack. *Journal of Sound and Vibration*, *332*(16), 3881–3892. doi: https://doi.org/10.1016/j.jsv.2013.02.031

Guo, D., & Peng, Z. (2007, nov). Vibration analysis of a cracked rotor using hilbert–huang transform. *Mechanical Systems and Signal Processing*, *21*(8), 3030–3041. doi: https://doi.org/10.1016/j.ymssp.2007.05.004

Imam, I., Azzaro, S. H., Bankert, R. J., & Scheibel, J. (1989, jul). Development of an on-line rotor crack detection and monitoring system. *Journal of Vibration and Acoustics*, *111*(3), 241–250. doi: 10.1115/1.3269848

Ince, T., Kiranyaz, S., Eren, L., Askar, M., & Gabbouj, M. (2016, nov). Real-time motor fault detection by 1-d convolutional neural networks. *IEEE Transactions on Industrial Electronics*, *63*(11), 7067–7075. doi: 10.1109/TIE.2016.2582729

Jiang, X., Wang, F., Zhao, H., Xu, S., & Lin, L. (2020, nov). Novel orbit-based CNN model for automatic fault identification of rotating machines. *Annual Conference of the PHM Society*, *12*(1), 7. doi: 10.36001/phmconf.2020.v12i1.1147

Khan, A., Ko, D.-K., Lim, S. C., & Kim, H. S. (2019, mar). Structural vibration-based classification and prediction of delamination in smart composite laminates using deep learning neural network. *Composites Part B: Engineering*, *161*, 586–594. doi: 10.1016/j.compositesb.2018.12.118

Krizhevsky, A., Sutskever, I., & Hinton, G. E. (2012). Imagenet classification with deep convolutional neural networks. In F. Pereira, C. Burges, L. Bottou, & K. Weinberger (Eds.), *Advances in neural information processing systems* (Vol. 25). Curran Associates, Inc. Retrieved from https://proceedings.neurips.cc/paper_files/paper/2012/file/c399862d3b9d6b76c8436e924a68c45b-Paper.pdf

Krizhevsky, A., Sutskever, I., & Hinton, G. E. (2017, may). ImageNet classification with deep convolutional neural networks. *Communications of the ACM*, *60*(6), 84–90. doi: 10.1145/3065386

Lecun, Y., Bottou, L., Bengio, Y., & Haffner, P. (1998). Gradient-based learning applied to document recognition. *Proceedings of the IEEE*, *86*(11), 2278–2324. doi: 10.1109/5.726791

Li, B., Zhang, C., & He, Z. (2012, sep). HHT-based crack identification method for start-up rotor. *Frontiers of Mechanical Engineering*, *7*(3), 300–304. doi: https://doi.org/10.1007/s11465-012-0328-1

Lin, L., & Chu, F. (2012, jan). HHT-based AE characteristics of natural fatigue cracks in rotating shafts. *Mechanical Systems and Signal Processing*, *26*, 181–189. doi: https://doi.org/10.1016/j.ymssp.2011.07.017

Lin, M., Chen, Q., & Yan, S. (2013). Network in network. doi: 10.48550/arXiv.1312.4400

Mohamad, T. H., Abbasi, A., Kim, E., & Nataraj, C. (2021, jun). Application of deep CNN-LSTM network to gear fault diagnostics. doi: 10.1109/ICPHM51084.2021.9486591

Mohamad, T. H., & Nataraj, C. (2020, may). Fault identification and severity analysis of rolling element bearings using phase space topology. *Journal of Vibration and Control*, *27*(3-4), 295–310. Retrieved from https://doi.org/10.36001/phmconf.2017.v9i1.2382 doi: 10.1177/1077546320926293

Mohamad, T. H., Nazari, F., & Nataraj, C. (2019, jun). A review of phase space topology methods for vibration-based fault diagnostics in nonlinear systems. *Journal of Vibration Engineering &amp ; Technologies*, *8*(3), 393–401. doi: 10.1007/s42417-019-00157-6

Nelson, H. D., & Nataraj, C. (1986, apr). The dynamics of a rotor system with a cracked shaft. *Journal of Vibration and Acoustics*, *108*(2), 189–196. doi: https://doi.org/10.1115/1.3269321

Patel, T. H., & Darpe, A. K. (2008). Influence of crack breathing model on nonlinear dynamics of a cracked rotor. *Journal of Sound and Vibration*, *311*(3), 953-972. Retrieved from https://www.sciencedirect.com/science/article/pii/S0022460X0700781X doi: https://doi.org/10.1016/j.jsv.2007.09.033

Raghu, S., Sriraam, N., Temel, Y., Rao, S. V., & Kubben, P. L. (2020, apr). EEG based multi-class seizure type classification using convolutional neural network and transfer learning. *Neural Networks*, *124*, 202–212. doi: 10.1016/j.neunet.2020.01.017

Samadani, M., Kwuimy, C. A. K., & Nataraj, C. (2016, aug). Characterization of the nonlinear response of defective multi-DOF oscillators using the method of phase space topology (PST). *Nonlinear Dynamics*, *86*(3), 2023–2034. doi: 10.1007/s11071-016-3012-x

Sekhar, A. S. (2005, sep). Identification of unbalance and crack acting simultaneously in a rotor system: Modal expansion versus reduced basis dynamic expansion. *Journal of Vibration and Control*, *11*(9), 1125–1145. doi: https://doi.org/10.1177/1077546305042531

Shao, S., McAleer, S., Yan, R., & Baldi, P. (2019, apr). Highly accurate machine fault diagnosis using deep transfer learning. *IEEE Transactions on Industrial Informatics*, *15*(4), 2446–2455. doi: 10.1109/TII.2018.2864759

Shudeifat, M. A. A., & Nataraj, C. (2020). Post-resonance backward whirl in a jeffcott rotor with a breathing crack model. , 485–491. doi: https://doi.org/10.1007/978-3-030-34713-0_48

Wang, Z., & Oates, T. (2015). Imaging time-series to improve classification and imputation. doi: 10.48550/arXiv.1506.00327

Wang, Z., Oates, T., et al. (2015). Encoding time series as images for visual inspection and classification using tiled convolutional neural networks..

Wang, Z., & Yang, J. (2017). Diabetic retinopathy detection via deep convolutional networks for discriminative localization and visual explanation. doi: 10.48550/arXiv.1703.10757

Wu, B., Feng, S., Sun, G., Xu, L., & Ai, C. (2019, dec). Fine-grained fault recognition method for shaft orbit of rotary machine based on convolutional neural network. *Journal of Vibroengineering*, *21*(8), 2106–2120. doi: 10.21595/jve.2019.20359

Zheng, Y., Liu, Q., Chen, E., Ge, Y., & Zhao, J. L. (2014). Time series classification using multi-channels deep convolutional neural networks. , 298–310. doi: 10.1007/978-3-319-08010-9_33

Zhou, B., Khosla, A., Lapedriza, A., Oliva, A., & Torralba, A. (2016, jun). Learning deep features for discriminative localization. doi: 10.1109/CVPR.2016.319

Zhou, X., Jin, K., Shang, Y., & Guo, G. (2020, jul). Visually interpretable representation learning for depression recognition from facial images. *IEEE Transactions on Affective Computing*, *11*(3), 542–552. doi: 10.1109/TAFFC.2018.2828819